

Article

Electrochemotherapy with Bleomycin Supported by NIRF Imaging with Indocyanine Green (ICG)—In Vitro and In Vivo Case Study

Joanna Tunikowska ^{1,*}, Nina Rembiałkowska ², Olga Michel ³, Justyna Mączyńska ⁴, Agnieszka Antończyk ¹, Przemysław Prządka ¹, Zdzisław Kielbowicz ¹ and Julita Kulbacka ^{2,5,*}

- ¹ Department of Surgery, Faculty of Veterinary Medicine, Wrocław University of Environmental and Life Sciences, 50-356 Wrocław, Poland
- ² Department of Molecular and Cellular Biology, Faculty of Pharmacy, Wrocław Medical University, 50-367 Wrocław, Poland
- ³ Department of Cytobiochemistry, Faculty of Biotechnology, University of Wrocław, 50-137 Wrocław, Poland
- ⁴ Bioimaging Laboratory, Łukasiewicz Research Network—PORT Polish Center For Technology Development, 54-066 Wrocław, Poland
- ⁵ Department of Immunology, State Research Institute Centre for Innovative Medicine, 08410 Vilnius, Lithuania
- * Correspondence: joanna.tunikowska@upwr.edu.pl (J.T.); julita.kulbacka@umw.edu.pl (J.K.); Tel.: +48-7-1320-5351 (J.T.)

Abstract: Electrochemotherapy (ECT) with bleomycin has been effectively used in recent years to treat various skin tumors. Microsecond electric pulses significantly improve bleomycin (BLM) delivery and its anticancer potential. Up to now, we can determine electric field distribution in the targeted tissue, however, the distribution of the injected drug is still not well known. In this study, we propose the combination of indocyanine green (ICG) with bleomycin as a practical approach for ECT, enabling drug distribution control and detection. Normal skeletal muscle (L6) and fibrosarcoma (WEHI-164) cells were used for the viability evaluation by MTT assay after 24 and 72 h. Cells were exposed to the ESOP protocol alone and in combination with drugs. Additionally, visualization of the uptake of ICG and ICG + BLM supported by electroporation was performed by confocal microscopy. The mast cell tumor (MCTs) was diagnosed in the feline case. The mixture of ICG + BLM was injected into the tumor, and ECT was performed under near-infrared fluorescence imaging (NIRF). The obtained results indicate the safety of the used procedure in vitro and in vivo. ICG does not affect ECT protocols in vitro. No significant cell viability decrease was noted only in the case of WEHI-164 cells post-ECT. Moreover, it does not adversely affect the procedure; in the case of in vivo surgery, it helps to control the drug distribution before and after ECT and identify the sentinel lymph node.

Keywords: ESOP; bleomycin; indocyanine green; electrochemotherapy; NIRF



Citation: Tunikowska, J.; Rembiałkowska, N.; Michel, O.; Mączyńska, J.; Antończyk, A.; Prządka, P.; Kielbowicz, Z.; Kulbacka, J. Electrochemotherapy with Bleomycin Supported by NIRF Imaging with Indocyanine Green (ICG)—In Vitro and In Vivo Case Study. *Appl. Sci.* **2023**, *13*, 2027. <https://doi.org/10.3390/app13042027>

Academic Editors: Francesca Silvagno and Georges Wagnieres

Received: 7 December 2022

Revised: 1 February 2023

Accepted: 1 February 2023

Published: 4 February 2023



Copyright: © 2023 by the authors. Licensee MDPI, Basel, Switzerland. This article is an open access article distributed under the terms and conditions of the Creative Commons Attribution (CC BY) license (<https://creativecommons.org/licenses/by/4.0/>).

1. Introduction

1.1. Electrochemotherapy in Veterinary Oncology

Electrochemotherapy (ECT) is a local cancer treatment that has gained popularity in both human and veterinary oncology since European Standard Operating Procedures (ESOP) were published in 2006 [1]. The treatment consists of the combination of reversible electroporation with an appropriate electric pulse duration and electric field intensity leading to enhanced cytotoxicity of a chemotherapeutic drug inside the tumor [1,2]. The effectiveness of ECT was demonstrated in several tumor histotypes: melanoma, planum cell carcinoma, mast cell tumors, sarcomas, and others [3]. Most studies focus on the application of ECT in treating skin or head and neck tumors; however, new research also investigates its usefulness in internal organs, i.e., the liver and pancreas [4–7]. The way of drug administration can be achieved by local or systemic injection and depends

on the species, tumor size, and the type of chemotherapeutic [2,3,8]. One of the best-studied substances commonly used in ECT treatment is bleomycin (BLM). This is an antitumor antibiotic derived from *Streptomyces verticillus*, whose mechanism of action relies on sequence selective DNA binding and cleavage, resulting in DNA degradation [9]. BLM is a very potent cytotoxic drug once inside the cell; however, its large size and hydrophilic structure impede transport through the plasma membrane and hinder its high concentrations in the cytosol [10]. This limitation was conquered when the use of electroporation to increase BLM uptake into the cells was introduced [11]. Significant potentiation of BLM cytotoxicity can be obtained even in BLM-insensitive tumors [11]. The ECT is described as an easy and uncomplicated technique [12]. Among factors such as size, histotype, and exposure to previous oncological treatments, a good outcome relies on proper tumor infiltration with chemotherapeutics and electroporation of the whole tumor mass. Although the determination of electric field distribution in the targeted tissue may be predicted, the distribution of the injected drug is still difficult to detect. The authors of this study suggest combining indocyanine green (ICG) with bleomycin in ECT to attain control over drug distribution and allow for detection.

1.2. NIRF Coupling with ECT

One of the most popular imaging modes in biomedical sciences for visualizing cells and tissues is fluorescence imaging [13]. NIRF (near-infrared fluorescence) imagers provide information on the distribution of the weak (relative to white-light reflectance) fluorescence signal arising from the excited fluorescent agents within the surgical field [13–15]. A charge-coupled device camera captured and recorded the fluorescent signal [15]. As ICG works in the optical window of tissue, it is currently the most popular contrast used for in vivo fluorescence imaging [13]. There is a growing interest in using NIRF-ICG in oncology for identification and tumor assessment in human and veterinary medicine [13,16]. Coupling ECT with NIRF-ICG is a novel approach that can influence the outcome of the ECT treatment. The authors report that this is the first examination of the use of NIRF imaging during ECT treatment.

This study aimed to investigate the effect of electroporation of the normal and tumor cells with indocyanine green and a mixture of ICG with BLM on cell viability, accompanied by the clinical application of NIRF imaging for the ECT treatment in a feline in vivo case study.

2. Materials and Methods

2.1. In Vitro Study

2.1.1. Cell Line and Culture Conditions

In the current study, the following cell lines were used: the mouse fibrosarcoma cell line—WEHI-164, and normal rat skeletal muscle—L6. Both cell lines were purchased from ATCC[®]. Fibrosarcoma cells were maintained in RPMI 1640 culture medium (IITD, Wroclaw, Poland), skeletal muscle cells were grown using DMEM (Biological Industries) with 10% fetal bovine serum (FBS, Sigma-Aldrich, Burlington, MA, USA), antibiotic (penicillin/streptomycin; Sigma-Aldrich), and 1% L-glutamine, at 37 °C and 5% CO₂ in a 75 cm² plastic flask (Sarstedt, Germany). For the experiments, the cells were detached by trypsinization (Trypsin 0.025%, IITD, Wroclaw, Poland), which was further neutralized by a cell culture medium. Cells were passaged every 2–3 days and a day before the experiment. Before experiments, cells were detached by trypsin solution and washed with DPBS (Sigma-Aldrich, Poznan, Poland).

2.1.2. Electrochemotherapy (ECT) In Vitro Protocol

The electroporation of cells was performed in the electroporation cuvette with a 1 mm gap between electrodes (Biorad, Hercules, CA, USA). The standard ESOP protocol was used: 8 pulses of 100 μs duration, frequency 1 kHz, and electric field intensity 1300 V/cm. For pulse delivery, the ECM 830 Square Wave Electroporation System (BTX

Harvard Apparatus, Syngen Biotech, Wrocław, Poland) was used. After trypsinization and centrifugation (5 min, 1500 rpm) cells were resuspended in an SHM electroporation buffer [17,18] (HEPES based), and electroporated. Bleomycin (100 nM, Bleomedac, medac GmbH, Wedel, Germany) and indocyanine green (Verdye, Diagnostic Green, GmbH, Germany) (20 µg/mL) were used with electroporation as a single ECT drug treatment and mixture ECT treatment. Three technical repetitions were performed.

2.1.3. MTT Viability Assay

The MTT assay was used for the evaluation of the viability of cells after 24 or 72 h post-exposure to ECT. After electroporation, cells were resuspended in 96-well plates (Sarstedt, dist. Equimed, Poland) at a concentration of 2×10^4 . The MTT assay was used in our previous study, and a detailed procedure is described here [17]. The results were presented as a percentage compared to the untreated control cells. Experiments were repeated a minimum of three times in triplicate.

2.1.4. Intracellular Distribution of ICG by Confocal Microscopy

L6 and WEHI cells were seeded on cover microscopic slides (20 × 20 mm), placed in a 6-well plate (Sarstedt, Germany), and left overnight to adhere. Then, the ESOP protocol with ICG or ICG + BLM diluted in SHM electroporation buffer was performed by applying a contact plate electrode (Petri Dish 35 mm electrode—BTX, Syngen, Wrocław, Poland). Cells were fixed immediately post-treatment and after 24 h. For this purpose, the culture medium was removed, and the cover glasses were washed with PBS, fixed for 10 min in 4% paraformaldehyde (PFA), and washed with PBS. Slides were mounted in a fluorescence mounting medium (Sigma-Aldrich) containing DAPI (4,6-diamidino-2-phenylindole) for nuclei staining. The preparations were stored in the dark at 4 °C. The Leica TCS SP8 MP confocal laser scanning microscope (Leica Microsystems, Wetzlar, Germany) was used for imaging. For ICG detection, the following wavelengths were used: $\lambda_{exc} = 632$ nm and $\lambda_{em} = 835$ nm. Images were captured with a 20× (numerical aperture, NA—0.45) air objective and analyzed using Fiji ImageJ 1.53 t (ImageJ, USA). Maximum intensity projections (MIP) were generated from Z-stack images taken at 5µm intervals, using the following settings: 1024 × 1024 pixels, 8 speed, 4 averaging.

2.1.5. Statistical Analysis

The statistical analysis was performed using GraphPad Prism 8 (La Jolla, CA, USA). The results were analyzed by a non-parametric Kruskal–Wallis statistic test. Results were expressed as a median and range, where $p < 0.05$ was considered statistically significant.

2.2. *In Vivo*—Feline Case Study

A 14-year-old male domestic shorthair cat was referred to the veterinary center for removal of the mast cell tumor (MCTs) localized under the metatarsal pad of the left hind limb (Figure 1). The owner refused radical excision; therefore, alternative treatment with surgical excision of the mass supported by intraoperative ECT and removal of the sentinel lymph node was proposed. The owner signed the agreement consent for the proposed treatment. The study was approved based on consent issued by the Bioethical Committee of Wrocław University of Environmental and Life Sciences (Wrocław, Poland) no. 49/2020 and 50/2020 (valid for five years).

Surgery was conducted under short-infusion anesthesia and epidural analgesia. The cat was given dexmedetomidine (Dexdomitor, Orion Pharma, Espoo, Finland) at a dose of 40 mcg/kg intramuscularly in premedication. General anesthesia was induced using propofol (Propofol-Lipuro 1%, B. Braun Melsungen AG, Melsungen, Germany) until the desired level of unconsciousness was achieved. The cat was intubated with a cuffed endotracheal tube (internal diameter 4.0 mm) and was breathing spontaneously with oxygen-enriched air. Additional propofol was administered as a bolus of 1–2 mg/kg when

needed. The cat was clipped and washed to allow visualization of the suspected draining tracts, and the surgical field was routinely disinfected.

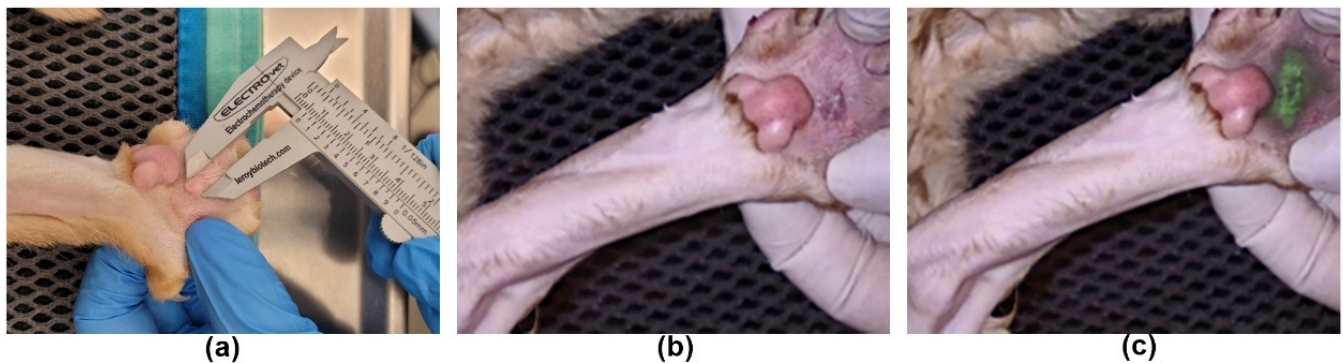


Figure 1. Visualization of the tumor: (a) Tumor mass before the ECT treatment, (b) tumor mass after infiltration with BLM-ICG, (c) tumor mass after infiltration with BLM-ICG with fluorescence green overlay.

The visualization of the BLM-ICG fluorescence was conducted with VS3 Iridium™ (Philadelphia, PA, USA). The excitation source is a laser tuned in the NIR range ($\lambda_{exc} = 805$ nm, and $\lambda_{em} = 835$ nm) with an incident excitation power of 11 mW/cm^2 at 30 cm from the tissue (Figure 1b,c). The level of the infrared signal (IR) captured by the camera from the surgical field was visible on the screen as a scale of IR intensity. The absolute intensity of the IR signal was visible at a given point (Base Point) on the screen ranging from 0 to 255 (Figure 2). The relative intensity of the IR signal at user-specified points was calculated by the system with reference to the base point (in %). The tumor mass was injected with bleomycin (Bleomedac, medac GmbH, Germany) at a dose of 1 mL/cm^3 of the tumor mass mixed with 0.1 mL of indocyanine green 5 mg/mL (Verdye, Diagnostic Green, GmbH, Kirchheim bei München, Germany) and exposed to the ESOPE protocol.



Figure 2. The screenshot from the NIRF imaging after ECT treatment shows the fluorescence of ICG in three modalities—IR, color fused, and green overlay, and the scale with strength of the IR signal.

For pulse delivery, the ELECTROcell B15 (Leroy Biotech, Saint-Orens-de-Gameville, France) and an applicator with a contact L-shape electrode 10 mm gap was used. A standard ESOPE pulsing protocol was employed. The electroporation was made immediately after drug administration, directly on the tumor mass and at a distance ranging from 5–15 mm. After ECT, the tumor mass was excised routinely with a CO₂ laser (Aesculight, Bothell, WA, USA) using 0.25 mm spot size, working in super pulse mode and 10 W of power output. Due to finding the draining node, the lymphatics were followed until the point at which they were no longer visible in the skin. Then, the suspected lymph node exhibiting fluorescence was removed. The wounds were sutured with monofilament nonabsorbable suture material (Figure 2b). Tumor tissue and lymph node were directed for CLSM (Leica TCS SP8 MP) imaging, similarly as for the *in vitro*. For the ICG detection, the following wavelengths were used $\lambda_{exc} = 638$ nm and $\lambda_{em} = 660$ –788 nm. Images were captured with a 25× (numerical aperture, NA 0.95) water objective. Maximum intensity projections (MIP) were generated from Z-stack images taken at 3µm intervals, using the following settings: 512 × 512 pixels, 8000 Hz speed, 16 line averaging. Multiphoton-induced second-harmonic generation and two-photon excitation enabled label-free imaging of collagen.

Application of the super-oxidized solution Microdacyn 60 hydrogel[®] (Kikgel, Ujazd, Poland) twice daily was recommended to the owner. Robenacoxib, in a dose of 1 mg/kg, was given once daily for ten days after the surgery. Necrotic tissue debridement was undertaken two weeks after the ECT and the wounds were left for second-intention healing under aqua-gel dressings.

3. Results

3.1. *In Vitro* Studies

Figure 3 shows the ECT effect on cancer and normal cells. As a chemotherapeutic drug, bleomycin was used. Additionally, ICG—a diagnostic marker, was used to determine its cytotoxic effect when applied simultaneously with the ECT protocol. In the case of L6 cells, which are normal skeletal muscle, a similar effect was observed but with weaker intensity, i.e., ca. 60% cells' viability after 24 h post-ECT + BLM or ECT + BLM + ICG (Figure 3a), and 52% after 72 h post-ECT + BLM + ICG (Figure 3b). The results show that WEHI-164 cell viability decreased to ca. 57% after ECT with bleomycin, independently of the time post-experiment. In the case of ECT with BLM and ICG, cells' viability decreased to 48% after 24 h (Figure 3c) and 42% after 72 h (Figure 3d). ECT with ICG only induced a 13% decrease after 72 h in normal cell viability, which was not significant. BLM and ICG or their mixture without electroporation did not significantly affect cell viability.

Figure 4 demonstrates the intracellular distribution of ICG in L6 and WEHI cells. ICG was delivered to cells in standard incubation protocol or via electroporation (ESOPE). Additionally, ICG was mixed with bleomycin. The results indicate that the ESOPE protocol improved ICG and ICG + BLM transport to both exposed cell lines. The highest ICG and ICG + BLM uptake was observed directly after exposure to the electric pulses. The intensity of the fluorescent signal was comparable in both cell lines. In the case of cells that were not exposed to electroporation, ICG or ICG + BLM delivery was traceable and insignificant. There was not a significant enhancement of the fluorescent signal in WEHI cells after 24 h. Figure 4c shows the analysis of the fluorescent signal from CLSM images. We can observe the most intensive increase in RFU in protocols combined with electroporation.

3.2. *In Vivo*—Feline Case Study

The fluorescence of the ICG in the mixture with BLM was preserved. During the procedure, the fluorescence of BLM-ICG was visible at the moment of the intratumoral injection and after electroporation. Fluorescence imaging allowed for the intraoperative visualization of the BLM-ICG in the infiltrated tissue within 6 s after drug deposition into the tissue. The fluorescence in the sentinel lymph node was visible within 4 min of the injection. The maximum relative intensity level reached 92% and was visible 9 min after the BLM-ICG injection (Figures 2 and 5). After the drug mixture injection, the ESOPE

protocol was performed as described in Section 2.2. The BLM-ICG mixture was visible during electroporation. The fluorescence of the contaminated gloves, the patient's skin, and surgical drapes with BLM-ICG mixture were visible under the NIRF imaging camera. Histopathologic examination confirmed clean margin resection of low-grade mastocytoma and infiltration of the popliteal lymph node with mast cells. Figure 6 shows the ICG accumulation in the tumor tissue received from the resection and from the lymph node. We can see a strong fluorescent ICG signal in the tumor tissue exposed to ECT. Interestingly, we also detected fluorescent ICG signals in lymph nodes, which were not treated by ECT. Thus, it confirms that the mixture of BLM and ICG was also delivered there.

Further observations revealed that complete healing was obtained 5 weeks after the surgery. The cat was controlled after five months post-ECT procedure, and no recurrences were observed.

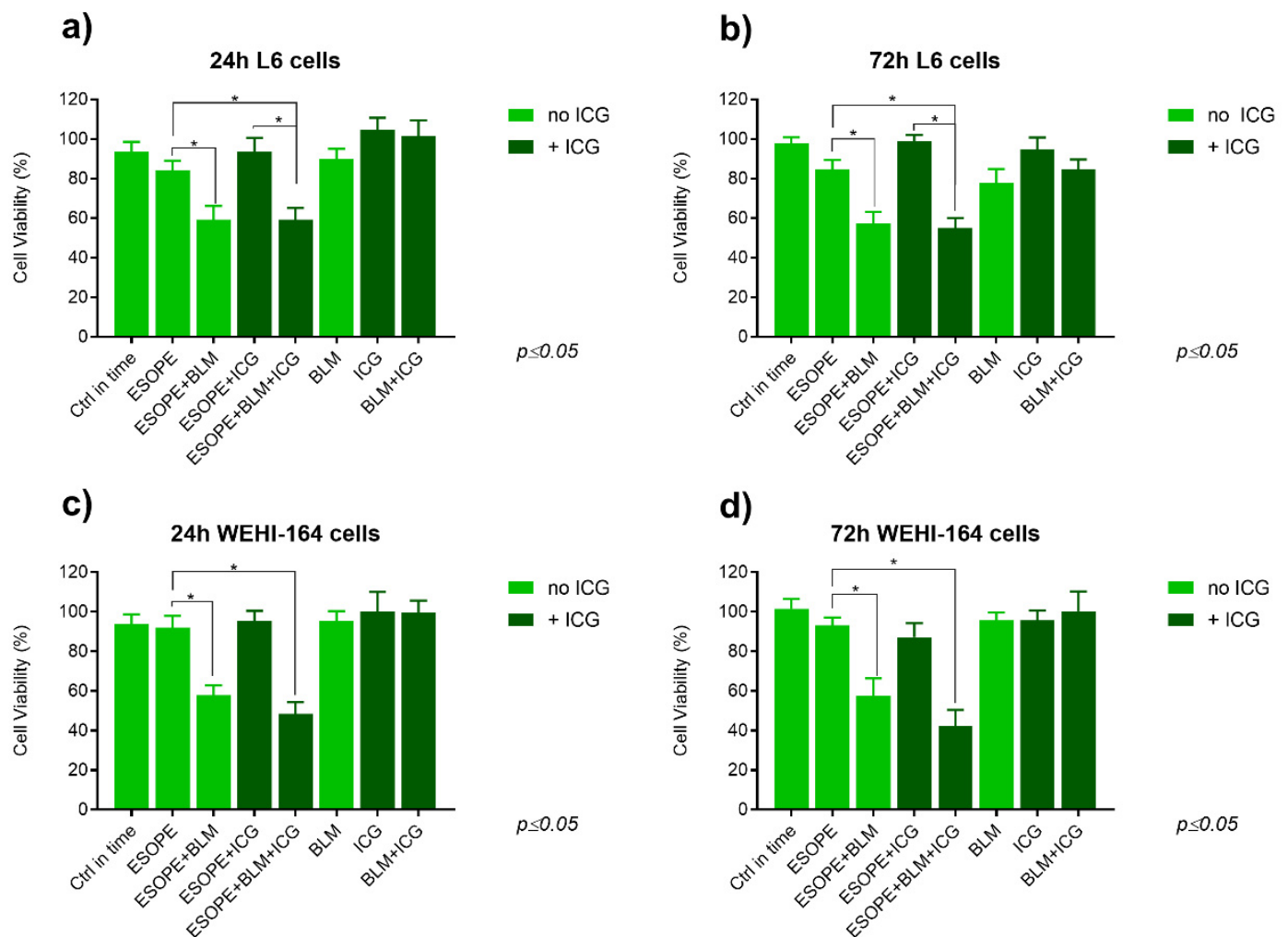
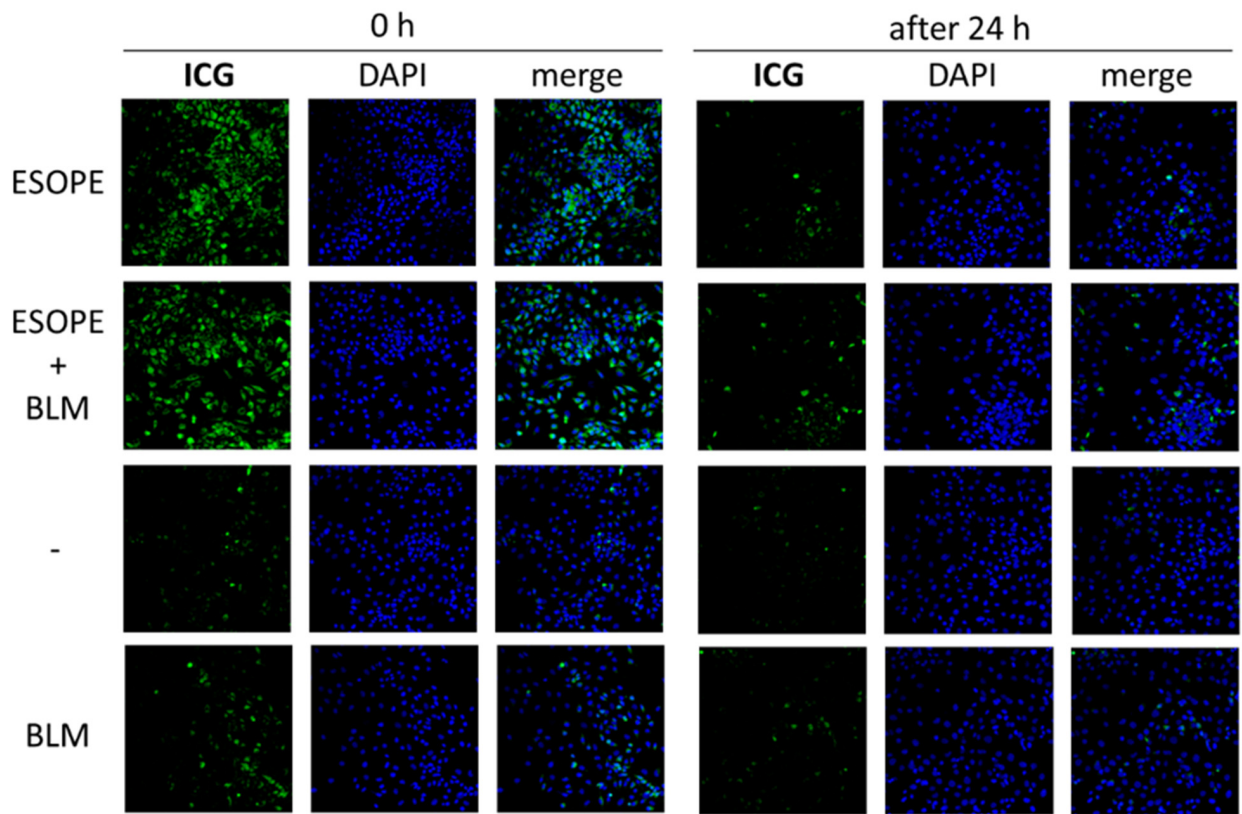


Figure 3. Cell viability by MTT assay. The effects of ECT with BLM and ICG in L6 cells after 24 (a) and 72 h (b). The effects of ECT with BLM and ICG in WEHI-164 cells after 24 (c) and 72 h (d). BLM—bleomycin (100 nM), ICG—(indocyanine green, 20 $\mu\text{g}/\text{mL}$), ESOPE—standard electroporation protocol for ECT. * $p \leq 0.05$ corresponds to statistically significant.

(a) L6



(b) WEHI

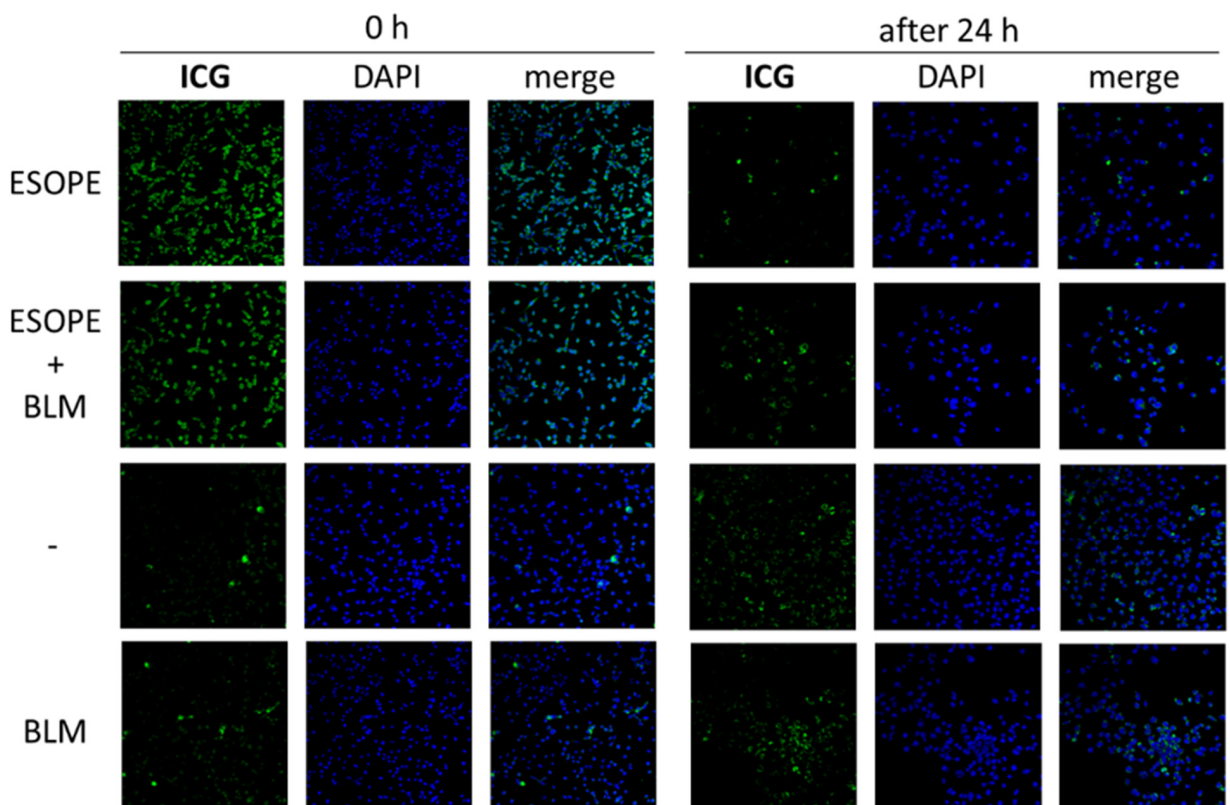


Figure 4. Cont.

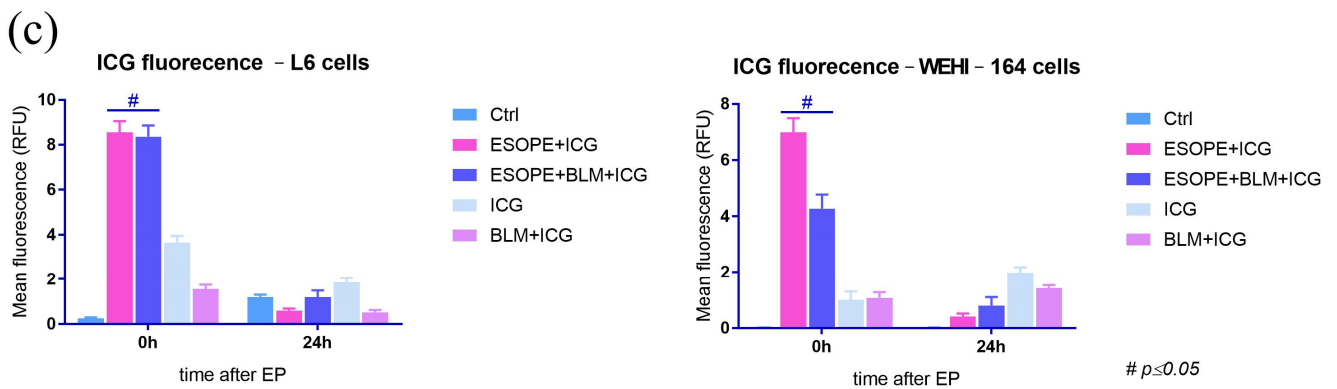


Figure 4. Intracellular visualization of ICG distribution combined with BLM and ESOPE protocol in L6 cells (a) and WEHI-164 cells (b), directly post-treatment (0 h) and after 24 h. (c) The analysis of the fluorescent signal in L6 and WEHI-164 cells from CLSM images by ImageJ software BLM—bleomycin (100 nM), ICG—(indocyanine green, 20 µg/mL), ESOPE—standard electroporation protocol for ECT, RFU—relative fluorescence units. # $p \leq 0.05$ corresponds to statistically significant.

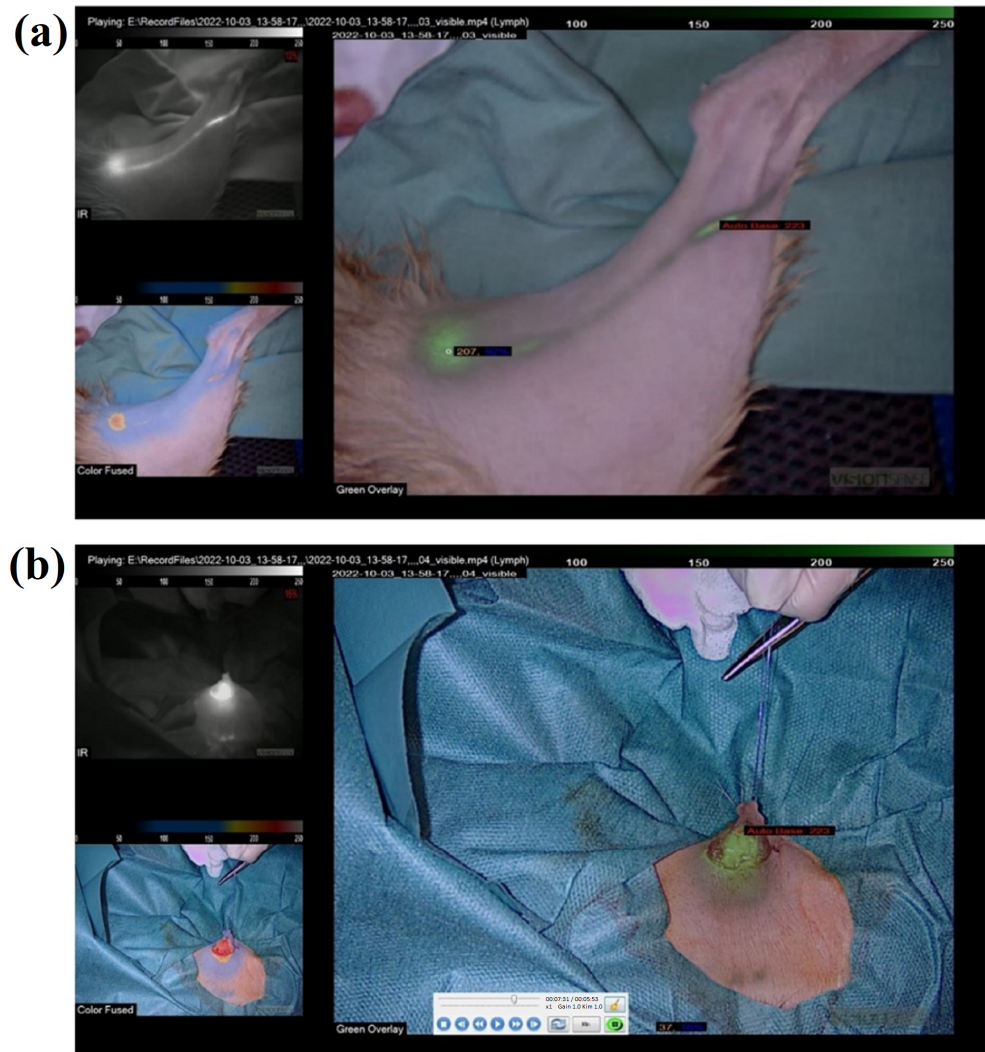


Figure 5. The screenshot from the NIRS imaging system after ECT treatment (a) fluorescence of the BLM-ICG in the lymphatics and popliteal lymph node before excision. (b) Fluorescence of the popliteal lymph node during surgical removal.

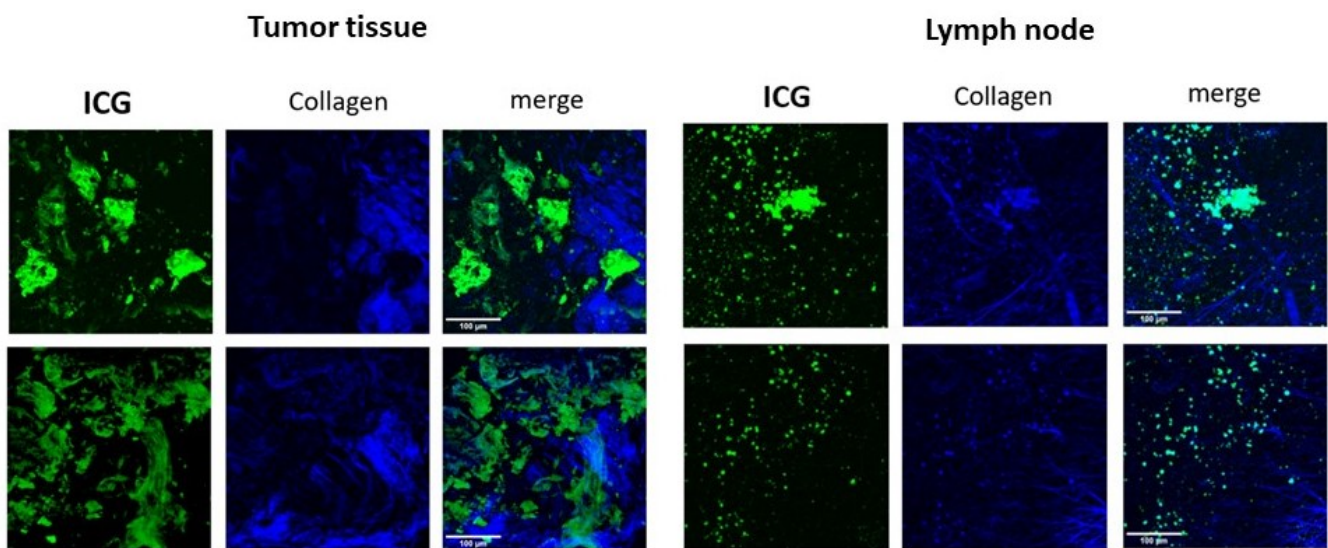


Figure 6. ICG distribution in tumor tissue and lymph node of the feline, where lymph nodes were not exposed to ECT (unfixed tissue, 24 h after resection) ICG—(indocyanine green, 20 µg/mL).

4. Discussion

The features of NIR-excited dyes are also effectively used in photodynamic protocols, where this cyanine fits perfectly into the therapeutic window of biological tissues (700–900 nm) [19]. NIRF-based imaging is an effective tool that enables early cancer detection and treatment [20,21]. Recently, NIRF dyes are also incorporated for multifunctional protocols that are combined with chemotherapy [22], photodynamic therapy [23], or photothermal therapy [19]. In this study, we have demonstrated for the first time the usage of indocyanine green (ICG) with electrochemotherapy (ECT) with bleomycin (BLM). The idea behind a certain decision was influenced by the lack of control over the distribution of drugs during ECT treatment. ECT-based protocols mostly use non-fluorescent chemotherapeutics such as bleomycin or cisplatin [24–26]. In our study, various models *in vitro* and *in vivo* were used. Fibrosarcoma (used *in vitro*) and mast cell tumor (MCT) (feline case) are both malignant tumors that can originate from connective tissue, so it is possible to compare them to some extent. Moreover, *in vitro* validation allows you to check the toxicity of the therapy before applying it to the patient. Our results *in vitro* reveal that ICG can be safely combined with bleomycin and does not affect the efficacy of BLM. The decision on additional ECT in this patient's case was based on inconclusive cytology results, the clinical appearance of the mass, and the owner's capability for only one-time treatment. Additionally, the presented case study on the domestic cat confirms the safety and effectiveness of the ICG-BLM-ECT protocol.

The advantage of combining BLM with ICG is spatial and temporal visualization of the electroporation field. ICG has several clinically valuable properties, including a good signal-to-noise ratio and operation in optical tissue windows, enabling deep imaging [13]. Both BLM and ICG are characterized by good solubility in water as well as low toxicity. ICG dose—60 to 80 mg/kg, caused 50% mortality (LD₅₀) in mice following intravenous administration [27], whereas LD₅₀ of intraperitoneally administered bleomycin ranged from 72 to 520 mg/kg in rats [9,10]. In the context of ECT, some (bio)chemical differences between ICG and BLM may influence their behavior during the electroporation procedure. ICG molecular weight is 774.97 g/mol, with an average size from 3 to 300 nm [28], whereas bleomycin, a complex mixture of related glycolipopeptides with a larger molecular weight (1415.56 g/mol), can also range from a few nanometers to tens of nanometers, depending on factors such as its conformation and hydration state. It was demonstrated that electric pulses induced an increased cell permeability and might augment the cytotoxicity of bleomycin by several 100-fold [29], which suggests that the compound size is not the

critical aspect of ECT efficacy. Due to its hydrophilic character, bleomycin easily penetrates through pores created during electroporation. ICG on the other hand possesses both hydrophilic and lipophilic properties and may interact with cellular phospholipids [30] and proteins [31]. The ability of ICG to bind to serum proteins was used by Tummers et al. who aimed to detect ovarian cancer metastases based on a resulting enhanced permeability and retention of ICG [32]. Unfortunately, this approach appeared ineffective due to low specificity—all malignant lesions were detected, and a high-false positive signal was also present. In our study, we expected the tumor penetration by ICG to be similar or worse compared to BLM. Thus, we mixed both drugs and our results indicate an increased ICG uptake after electroporation in cells and in the tumor tissue. The most interesting was the detectable fluorescent ICG signal in lymph nodes, which were not electroporated. Thus, it suggests that BLM also can reach lymph node tissue. Additional comprehensive studies, including analysis of the cellular localization of ICG and BLM, are necessary to support the findings.

In theory, the problem of uneven tissue distribution of BLM and ICG could be solved by encapsulating both compounds inside a nanocarrier. Such an approach was explored in several studies, most of which used ICG as a photosensitizer. For example, Zhu et al. established a drug delivery system consisting of ICG and doxorubicin encapsulated in microvesicles to obtain effective synergistic photochemotherapy toward cervical cancer [33]. ICG was also used to solubilize the hydrophobic drug SN38 eliciting synergistic phototoxic and cytotoxic effects *in vitro* and *in vivo* against human glioblastoma cells and breast cancer cells upon NIR irradiation [34]. Importantly, ICG was combined with cisplatin (another standard drug used in ECT) within a hydrazided hyaluronan/cisplatin/ICG coordination nano-prodrug, which appeared to be highly effective toward hepatocellular carcinoma [32]. However, it has to be noted that lipid carriers may not be delivered with the standard ESOPE protocol due to their instability in the electric field. On the other hand, lipid nanoparticles had been successfully delivered to colon cancer cells using electric pulses of millisecond duration [35]. Overall, the ECT protocol with the modification involving the fusion of ICG and chemotherapeutics entrapped in nanocarriers seems to be a promising approach to trigger synergistic cytotoxic and phototoxic antitumor effects.

One of the main applications of NIRF-ICG imaging is mapping the sentinel lymph nodes [3,13,36,37]. In our study, we noticed fluorescence in the region of the popliteal node a few minutes after the injection. Histopathological examination confirmed that the fluorescent signal was from the regional lymph node. Our observation is in agreement with the clinical studies of Arz et al. concluding that NIR lymph node mapping was a safe procedure that helped identify and resect normal-sized metastatic lymph nodes in a cat with MCT [38]. Combining ICG with bleomycin for ECT has a theranostic implication—allowing both treatment of the primary tumor with additional visualization of the sentinel node draining from the region of interest.

Electrochemotherapy (ECT) is an effective local therapy for cutaneous tumors in human and veterinary patients. However, according to the National Institute for Occupational Safety and Health, handling cytotoxic drugs has been classified as an occupational health hazard [39,40], thus all procedures that involve cytostatic drugs are a risk; such drugs are carcinogenic, mutagenic, teratogenic, and abortifacient, increasing the risk of stillbirth [39]. The administration of the cytotoxic drug may be controlled by using well-established guidelines for chemotherapy administration protocols, but the guidelines during intratumoral application are still complicated and sometimes challenging. Our experience in IT injections in the case of tumor masses that are dense in structure and have more fibrous tissue indicates the spillage usually occurs after a backward flush of the drug; on the other hand, in soft tumors, the spillage usually occurs through pores and holes in the necrotizing mass. In both cases, the contamination risk may be elevated whether the treatment is simultaneous ECT and surgical excision. We hypothesize that adding the ICG to the BLM may allow for fast visualization of the possible drug leakage and contaminants during the ECT. In this study, the tumor mass was small, and accidental drug outflow was noted.

Thus, as we can state, the long-term benefits of NIRF imaging applications are not only for the patient during the procedure but also for the personnel's safety during ECT with IT injection.

In our opinion, further investigations on NIRF imaging in ECT treatment might focus on its influence on the following:

1. The reduction of risk of intraoperative contamination of the personnel with the cytostatic during intertumoral injections with cytostatic during ECT.
2. The treatment outcome by enhancing the tumor margins and its infiltration of the cytotoxic drug.
3. The intraoperative visualization of the draining lymph node and its electroporation with or without additional application of the cytostatic.

The main limitations of the study, as highlighted by other authors, include the camera-to-tissue distance and camera angle [41]. Additionally, the depth of the tissue also limits the method, making it suitable only for the treatment of surface tumors or for laparoscopic treatment.

5. Conclusions

ECT is a promising method in veterinary that can be used for the effective treatment of sarcoma, fibrosarcoma, or fibromas. Despite the high effectiveness of this method, efforts are ongoing to find new solutions that will speed up the procedure and enable more accurate treatment of patients. Our study demonstrated that the combination of NIRF-ICG imaging in ECT could provide a valuable tool in electroporation-based therapies and ensure the safety of drug delivery. However, ECT supported by NIRF-ICG requires further and comprehensive investigations.

Author Contributions: Conceptualization, J.T. and Z.K.; in vitro methodology, N.R. and J.K.; in vivo methodology, J.T., A.A. and Z.K.; investigation, J.T.; writing—original draft preparation, J.T.; writing—review and editing, J.T., O.M., J.K. and P.P.; visualization J.M. and J.K. All authors have read and agreed to the published version of the manuscript.

Funding: IA/SP/489694/2021 “Investments in Science” Polish Ministry of Education and Science.

Institutional Review Board Statement: Not applicable.

Informed Consent Statement: Not applicable.

Data Availability Statement: Data is contained within the article.

Conflicts of Interest: The authors declare no conflict of interest.

References

1. Marty, M.; Sersa, G.; Garbay, J.R.; Gehl, J.; Collins, C.G.; Snoj, M.; Billard, V.; Geertsen, P.F.; Larkin, J.O.; Miklavcic, D.; et al. Electrochemotherapy—An Easy, Highly Effective and Safe Treatment of Cutaneous and Subcutaneous Metastases: Results of ESOPE (European Standard Operating Procedures of Electrochemotherapy) Study. *Eur. J. Cancer Suppl.* **2006**, *4*, 3–13. [[CrossRef](#)]
2. Spugnini, E.P.; Baldi, F.; Mellone, P.; Feroce, F.; D'Avino, A.; Bonetto, F.; Vincenzi, B.; Citro, G.; Baldi, A. Patterns of Tumor Response in Canine and Feline Cancer Patients Treated with Electrochemotherapy: Preclinical Data for the Standardization of This Treatment in Pets and Humans. *J. Transl. Med.* **2007**, *5*, 48. [[CrossRef](#)]
3. Nemec, A.; Milevoj, N.; Lamprecht Tratar, U.; Serša, G.; Čemažar, M.; Tozon, N. Electroporation-Based Treatments in Small Animal Veterinary Oral and Maxillofacial Oncology. *Front. Vet. Sci.* **2020**, *7*, 575911. [[CrossRef](#)] [[PubMed](#)]
4. Mali, B.; Gorjup, V.; Edhemovic, I.; Breclj, E.; Cemazar, M.; Sersa, G.; Strazisar, B.; Miklavcic, D.; Jarm, T. Electrochemotherapy of Colorectal Liver Metastases—An Observational Study of Its Effects on the Electrocardiogram. *BioMedical Eng. OnLine* **2015**, *14*, S5. [[CrossRef](#)]
5. Trovšek, B.; Djokić, M.; Čemažar, M.; Serša, G. New Era of Electrochemotherapy in Treatment of Liver Tumors in Conjunction with Immunotherapies. *World J. Gastroenterol.* **2021**, *27*, 8216–8226. [[CrossRef](#)] [[PubMed](#)]
6. Girelli, R.; Prejanò, S.; Cataldo, I.; Corbo, V.; Martini, L.; Scarpa, A.; Claudio, B. Feasibility and Safety of Electrochemotherapy (ECT) in the Pancreas: A Pre-Clinical Investigation. *Radiol. Oncol.* **2015**, *49*, 147–154. [[CrossRef](#)]
7. Rudno-Rudzińska, J.; Kielan, W.; Guziński, M.; Płochocki, M.; Kulbacka, J. The First Study of Irreversible Electroporation with Calcium Ions and Chemotherapy in Patients with Locally Advanced Pancreatic Adenocarcinoma. *Appl. Sci.* **2020**, *10*, 5163. [[CrossRef](#)]

8. Campana, L.G.; Miklavčič, D.; Bertino, G.; Marconato, R.; Valpione, S.; Imarisio, I.; Dieci, M.V.; Granziera, E.; Cemazar, M.; Alaibac, M.; et al. Electrochemotherapy of Superficial Tumors—Current Status: Basic Principles, Operating Procedures, Shared Indications, and Emerging Applications. *Semin. Oncol.* **2019**, *46*, 173–191. [CrossRef]
9. Moore, C.W. Bleomycin. *Encycl. Mol. Biol.* **2002**. [CrossRef]
10. Mir, L.M.; Tounekti, O.; Orłowski, S. Bleomycin: Revival of an Old Drug. *Gen. Pharmacol. Vasc. Syst.* **1996**, *27*, 745–748. [CrossRef]
11. Ema Ar, M.; Miklav, D.; Ser, G. Intrinsic Sensitivity of Tumor Cells to Bleomycin as an Indicator of Tumor Response to Electrochemotherapy. *Jpn. J. Cancer Res.* **1998**, *89*, 328–333.
12. Tellado, M.N.; Maglietti, F.H.; Michinski, S.D.; Marshall, G.R.; Signori, E. Electrochemotherapy in Treatment of Canine Oral Malignant Melanoma and Factors Influencing Treatment Outcome. *Radiol. Oncol.* **2020**, *54*, 68–78. [CrossRef]
13. Alander, J.T.; Kaartinen, I.; Laakso, A.; Pätilä, T.; Spillmann, T.; Tuchin, V.v.; Venermo, M.; Välisuo, P. A Review of Indocyanine Green Fluorescent Imaging in Surgery. *Int. J. Biomed. Imaging* **2012**, *2012*, 7. [CrossRef] [PubMed]
14. Favril, S.; Abma, E.; Stock, E.; Devriendt, N.; Goethem, B.v.; Blasi, F.; Brioschi, C.; Polis, I.; de Cock, H.; Miragoli, L.; et al. Fluorescence-Guided Surgery Using Indocyanine Green in Dogs with Superficial Solid Tumours. *Vet. Rec.* **2020**, *187*, 273. [CrossRef] [PubMed]
15. DSouza, A.v.; Lin, H.; Henderson, E.R.; Samkoe, K.S.; Pogue, B.W. Review of Fluorescence Guided Surgery Systems: Identification of Key Performance Capabilities beyond Indocyanine Green Imaging. *J. Biomed. Opt.* **2016**, *21*, 080901. [CrossRef] [PubMed]
16. Wan, J. The Use of Near Infrared Fluorescence Imaging for Sentinel Lymph Node Mapping in Dogs. Ph.D. Thesis, University of Guelph, Guelph, ON, Canada, 2021.
17. Kulbacka, J.; Rembiałkowska, N.; Szewczyk, A.; Moreira, H.; Szyjka, A.; Girkontaitė, I.; Greła, K.P.; Novickij, V. The Impact of Extracellular Ca²⁺ and Nanosecond Electric Pulses on Sensitive and Drug-Resistant Human Breast and Colon Cancer Cells. *Cancers* **2021**, *13*, 3216. [CrossRef]
18. Novickij, V.; Rembiałkowska, N.; Kasperkiewicz-Wasilewska, P.; Baczyńska, D.; Rzechonek, A.; Błasiak, P.; Kulbacka, J. Pulsed electric fields with calcium ions stimulate oxidative alternations and lipid peroxidation in human non-small cell lung cancer. *Biochim. Biophys. Acta-Biomembr.* **2022**, *1864*, 184055. [CrossRef]
19. Shramova, E.I.; Kotlyar, A.B.; Lebedenko, E.N.; Deyev, S.M.; Proshkina, G.M. Near-Infrared Activated Cyanine Dyes As Agents for Photothermal Therapy and Diagnosis of Tumors. *Acta Nat.* **2020**, *12*, 2020. [CrossRef] [PubMed]
20. Li, Y.; Zhou, Y.; Yue, X.; Dai, Z. Cyanine Conjugates in Cancer Theranostics. *Bioact. Mater.* **2021**, *6*, 794–809. [CrossRef] [PubMed]
21. Borlan, R.; Focsan, M.; Maniu, D.; Astilean, S. Interventional NIR Fluorescence Imaging of Cancer: Review on Next Generation of Dye-Loaded Protein-Based Nanoparticles for Real-Time Feedback During Cancer Surgery. *Int. J. Nanomed.* **2021**, *16*, 2147. [CrossRef]
22. Jaiswal, S.; Dutta, S.B.; Nayak, D.; Gupta, S. Effect of Doxorubicin on the Near-Infrared Optical Properties of Indocyanine Green. *ACS Omega* **2021**, *6*, 34842–34849. [CrossRef] [PubMed]
23. Zhao, X.; Zhao, H.; Wang, S.; Fan, Z.; Ma, Y.; Yin, Y.; Wang, W.; Xi, R.; Meng, M. A Tumor-Targeting Near-Infrared Heptamethine Cyanine Photosensitizer with Twisted Molecular Structure for Enhanced Imaging-Guided Cancer Phototherapy. *J. Am. Chem. Soc.* **2021**, *143*, 20828–20836. [CrossRef]
24. Sersa, G.; Miklavcic, D.; Cemazar, M.; Rudolf, Z.; Pucihar, G.; Snoj, M. Electrochemotherapy in Treatment of Tumours. *Eur. J. Surg. Oncol.* **2008**, *34*, 232–240. [CrossRef] [PubMed]
25. Spugnini, E.P.; Baldi, A. Electrochemotherapy in Veterinary Oncology: From Rescue to First Line Therapy. In *Electroporation Protocols*; Humana Press: New York, NY, USA, 2014; pp. 247–256.
26. Cemazar, M.; Sersa, G. Recent Advances in Electrochemotherapy. *Bioelectricity* **2019**, *1*, 204. [CrossRef] [PubMed]
27. Patheon Italia S.P.A (Green LLC). Indocyanine Green. Available online: <https://www.drugs.com/pro/indocyanine-green> (accessed on 31 January 2023).
28. DeDora, D.J.; Suhrland, C.; Goenka, S.; Mullick Chowdhury, S.; Lalwani, G.; Mujica-Parodi, L.R.; Sitharaman, B. Sulfobutyl ether β -cyclodextrin (Captisol[®]) and methyl β -cyclodextrin enhance and stabilize fluorescence of aqueous indocyanine green. *J. Biomed. Mater. Res. Part B Appl. Biomater.* **2016**, *104*, 1457–1464. [CrossRef]
29. Gothelf, A.; Mir, L.M.; Gehl, J. Electrochemotherapy: Results of Cancer Treatment Using Enhanced Delivery of Bleomycin by Electroporation. *Cancer Treat. Rev.* **2003**, *29*, 371–387. [CrossRef]
30. Desmettre, T.; Devoisselle, J.M.; Mordon, S. Fluorescence Properties and Metabolic Features of Indocyanine Green (ICG) as Related to Angiography. *Surv. Ophthalmol.* **2000**, *45*, 15–27. [CrossRef]
31. Muckle, T.J. Plasma Proteins Binding of Indocyanine Green. *Biochem. Med.* **1976**, *15*, 17–21. [CrossRef]
32. Tummers, Q.R.J.G.; Hoogstins, C.E.S.; Peters, A.A.W.; de Kroon, C.D.; Baptist, J.; Trimbos, M.Z.; van de Velde, C.J.H.; Frangioni, J.v.; Vahrmeyer, A.L.; Gaarenstroom, K.N. The Value of Intraoperative Near-Infrared Fluorescence Imaging Based on Enhanced Permeability and Retention of Indocyanine Green: Feasibility and False-Positives in Ovarian Cancer. *PLoS ONE* **2015**, *10*, e0129766. [CrossRef]
33. Zhu, L.; Wang, C.; Pang, D.W.; Zhang, Z.L. Controlled Release of Therapeutic Agents with Near-Infrared Laser for Synergistic Photochemotherapy toward Cervical Cancer. *Anal. Chem.* **2019**, *91*, 6555–6560. [CrossRef]
34. Hou, G.; Qian, J.; Guo, M.; Xu, W.; Wang, J.; Wang, Y.; Suo, A. Hydrazided Hyaluronan/Cisplatin/Indocyanine Green Coordination Nanoprodruge for Photodynamic Chemotherapy in Liver Cancer. *Carbohydr. Polym.* **2022**, *276*, 118810. [CrossRef] [PubMed]

35. Kulbacka, J.; Pucek, A.; Kotulska, M.; Dubińska-Magiera, M.; Rossowska, J.; Rols, M.P.; Wilk, K.A. Electroporation and Lipid Nanoparticles with Cyanine IR-780 and Flavonoids as Efficient Vectors to Enhanced Drug Delivery in Colon Cancer. *Bioelectrochemistry* **2016**, *110*, 19–31. [[CrossRef](#)] [[PubMed](#)]
36. Favril, S.; Abma, E.; Blasi, F.; Stock, E.; Devriendt, N.; Vanderperren, K.; de Rooster, H. Clinical Use of Organic Near-Infrared Fluorescent Contrast Agents in Image-Guided Oncologic Procedures and Its Potential in Veterinary Oncology. *Vet. Rec.* **2018**, *183*, 354. [[CrossRef](#)] [[PubMed](#)]
37. Chiti, L.E.; Gariboldi, E.M.; Stefanello, D.; De Zani, D.; Grieco, V.; Nolff, M.C. Sentinel Lymph Node Mapping and Biopsy in Cats with Solid Malignancies: An Explorative Study. *Animal* **2022**, *12*, 3116. [[CrossRef](#)]
38. Arz, R.; Seehusen, F.; Meier, V.S.; Nolff, M.C. Indocyanine-based near-infrared lymphography for real-time detection of lymphatics in a cat with multiple mast cell tumours. *JFMS Open Rep.* **2022**, *8*, 20551169221074960. [[CrossRef](#)]
39. Smith, A.N.; Klahn, S.; Phillips, B.; Parshley, L.; Bennett, P.; Flory, A.; Calderon, R. ACVIM Small Animal Consensus Statement on Safe Use of Cytotoxic Chemotherapeutics in Veterinary Practice. *J. Vet. Intern. Med.* **2018**, *32*, 904–913. [[CrossRef](#)]
40. Howard, J. Revised Document Posted: NIOSH List of Antineoplastic and Other Hazardous Drugs in Healthcare Settings 2012. *Fed. Regist.* **2012**, *77*, 41190.
41. Serra-Aracil, X.; García-Nalda, A.; Serra-Gómez, B.; Serra-Gómez, A.; Mora-López, L.; Pallisera-Lloveras, A.; Lucas-Guerrero, V.; Navarro-Soto, S. Experimental study of the quantification of indocyanine green fluorescence in ischemic and non-ischemic anastomoses, using the SERGREEN software program. *Sci. Rep.* **2022**, *12*, 13120. [[CrossRef](#)]

Disclaimer/Publisher's Note: The statements, opinions and data contained in all publications are solely those of the individual author(s) and contributor(s) and not of MDPI and/or the editor(s). MDPI and/or the editor(s) disclaim responsibility for any injury to people or property resulting from any ideas, methods, instructions or products referred to in the content.